Direct imaging of a laser mode via midinfrared near-field microscopy

Virginie Moreau, Michael Bahriz, and Raffaele Colombelli[a)]
Institut d'Electronique Fondamentale, Université Paris Sud, CNRS, 91405 Orsay, France

Paul-Arthur Lemoine and Yannick De Wilde[b)]
Laboratoire d'Optique Physique, ESPCI, CNRS-UPR A0005, 75005 Paris, France

Luke R. Wilson
Department of Physics and Astronomy, University of Sheffield, Sheffield S37RH, United Kingdom

Andrey B. Krysa
EPSRC National Centre for III-V Technologies, Department of Electronic and Electrical Engineering, University of Sheffield, Sheffield S1 3JD, United Kingdom

(Received 15 March 2007; accepted 18 April 2007; published online 16 May 2007)

Fabry-Pérot standing waves inside a midinfrared quantum cascade laser have been imaged using an apertureless scanning near-field optical microscope. The devices emit at $\lambda \approx 7.7\ \mu$m and they feature air-confinement waveguides, with the optical mode guided at the semiconductor-air interface. A consistent portion of the mode leaks evanescently from the device top surface and can be detected in the near field of the device. Imaging of the evanescent wave across a plane *parallel* to the device surface allows one to directly assess the effective light wavelength inside the laser material, yielding the effective index of refraction. Imaging across a plane *perpendicular* to the device surface allows one to directly measure the electric field decay length, which is found in excellent agreement with the numerical simulations. © *2007 American Institute of Physics*. [DOI: 10.1063/1.2738189]

The midinfrared (mid-IR, $5\ \mu\text{m} < \lambda < 30\ \mu$m) range of the electromagnetic spectrum is extremely important for sensing applications.[1] Most molecules of chemical and biological interest exhibit rotovibrational transitions in this wavelength range. Quantum cascade (QC) lasers,[2] devices based on intersubband (ISB) transitions in semiconductor heterostructures, cover these wavelengths and they are becoming integrated as mid-IR sources in commercial setups for trace gas detection. Alternative possibilities also exist for QC laser-based sensing systems. For instance, the devices could be made sensitive to a material/liquid which contacts the QC laser surface.[3–5]

Devices featuring an optical mode which leaks evanescently above the top surface have been implemented,[6,7] and they are perfectly suited to such applications.[4,5] A near-field diagnostic of these devices is important in view of understanding and optimizing their properties. They also provide an ideal playground for observations with mid-IR scanning near-field microscopes (SNOMs), offering the opportunity of imaging the light propagation *inside* a working (QC) laser.

SNOMs employ pulled optical fibers to achieve subwavelength resolution, but the development of mid-IR fibers is in its infancy. In contrast, the recently developed apertureless SNOM (a-SNOM) does not require any fiber. It operates across a broad spectral range extending from the visible to the microwaves[8–13] and it can be used in various configurations to map the near field produced by sources of different nature,[8–15] including visible/near-infrared lasers in operation.[11,12,15]

In this letter we report the direct imaging of the light confinement inside the cavity of a working mid-IR semiconductor laser. The result is obtained by near-field imaging of the evanescent electric field on the surface specifically designed[4,5] mid-IR ($\lambda \approx 7.7\ \mu$m) QC lasers. We observe the standing waves inside the Fabry-Pérot laser give an experimental estimate of the electric field intensity at the surface. These devices behave as generators *on demand* of intense evanescent electric fields, controlled by the injection current.

The combination of local microprobes with mid-IR semiconductor devices is rich for possible developments. Instead of using an external laser source (a CO_2 laser[16]), molecules could be deposited on the device top surface and observed with an a-SNOM. Also, the devices characterized here can generate and sustain surface-plasmon waves in the mid-IR if the top surface is metal coated.[4,17] In combination with an a-SNOM, they represent an ideal system to study *directly* the propagation, guiding, and control of long-wavelength surface plasmons on patterned/unpatterned surfaces.[18]

The QC laser devices for this work [Fig. 1(a)] have been grown by metal-organic vapor phase epitaxy and they operate in pulsed mode at room temperature (RT), at $\lambda \approx 7.7\ \mu$m. A detailed study of their behavior is reported in Ref. 4. A typical emission spectrum is shown in Fig. 1(b). A large fraction of the laser surface is left exposed (electric current is injected by two lateral metallic bands[6,7]), to allow an evanescent wave to leak into the air cladding above the device surface. Various QC laser ridge widths have been fabricated between 26 and 41 μm, with widths of the exposed regions typically 10 μm less than the etched width.

The principle of the a-SNOM measurements is sketched in Fig. 1(c), the setup and the measurement technique are detailed in Ref. 14, and a summary of the measurements on a typical device is reported in Fig. 2. The *far-field* light-current characteristic of the device (red squares) shows the onset of lasing at an injected current of 1.75 A, with the laser

[a)]Electronic mail: colombel@ief.u-psud.fr
[b)]Electronic mail: dewilde@optique.espci.fr

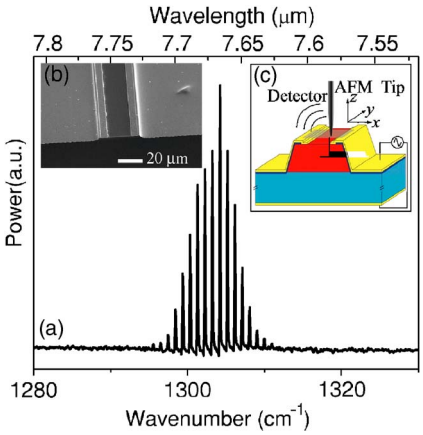

FIG. 1. (Color online) (a) Emission spectrum at RT of a laser device used for this work. The resonator length is 1.5 mm. The spectrum was acquired at a resolution of 0.125 cm^{-1}. The laser was operated with 50 ns pulses at 84 kHz repetition rate. The Fabry-Pérot modes are spaced of ≈0.97 cm^{-1}. Panel (b): SEM image of a typical device. Panel (c): Schematic of the a-SNOM setup (details in Ref. 14). The semitransparent gray rectangle corresponds to the typical area size scanned during a measurement run.

output detected from the facet in a conventional manner. The *near-field* light-current characteristic (black dots) is instead detected with the a-SNOM [Fig. 1(c)]. The position of the oscillating tip is kept fixed at the center of the ridge, where the active region is directly exposed to air, and the optical

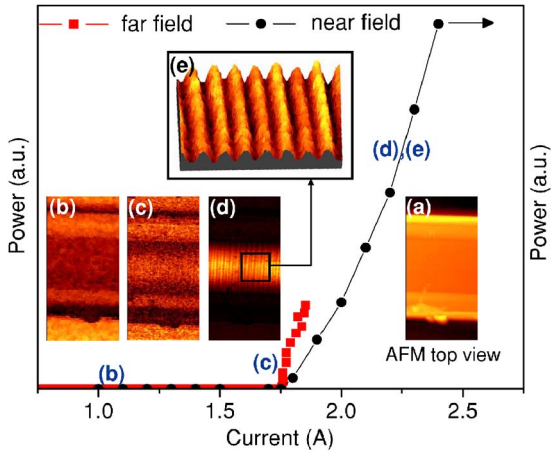

FIG. 2. (Color online) Main panel: Light-current characteristics of a typical device. Red dots: Far-field emission from the laser facet. The laser was operated with 50 ns pulses at 5 kHz repetition rate. Black dots: Near-field measurement (demodulated at the SNOM tip frequency f_{tip}.) The laser was operated with 50 ns pulses at 84 kHz repetition rate. Note that the *near-* and *far-field* signals appear at the same injection current. Panel (a): Atomic force microscopy view of the laser ridge. The scanning range is 30×60 μm^2, and it is identical for panels (a)–(d). The two lateral bright regions correspond to the lateral contact bands on top of the laser resonator, while the central, slightly darker region corresponds to the exposed semiconductor surface. The latter zone is where the evanescent electric field is expected to appear. Panel (b): Near-field measurement below threshold: only the thermal emission is present. Panel (c): Near-field measurement at threshold: the standing wave starts to emerge. Panel (d): Near-field measurement well above threshold. Panel (e): High resolution three-dimensional SNOM image of the standing wave. The same periodical structure is observed when demodulating the near-field signal at $2f_{tip}$ and $3f_{tip}$. The measured field at the device surface is thus purely evanescent, which results in the absence of background contribution from scattering centers located along the tip shaft far from the apex. For the same reason, the standing wave at the exposed surface of the ridge is also clearly observed in images obtained by demodulating the optical signal at the laser-pulse repetition frequency f_{laser}, while the tip scans the surface.

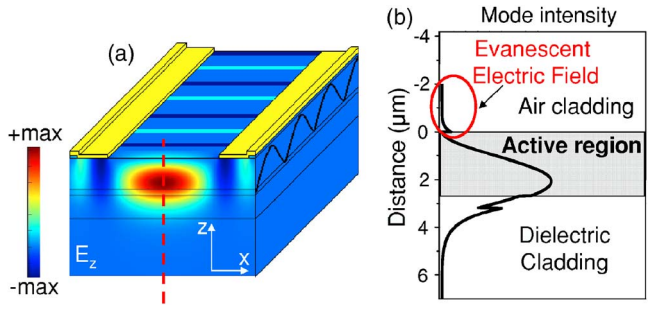

FIG. 3. (Color online) (a) Schematic view of the laser Fabry-Pérot resonator and its standing wave. A 2D simulation of the TM air-guided mode at $\lambda=7.7$ μm is superimposed on the facet (the E_z component is plotted). Note that only TM optical modes are expected, since the dipole of the ISB transitions is directed along z. This is in contrast with diode lasers that typically operate on transverse-electric modes. (b) One-dimensional simulation of the laser mode, corresponding to a cross section marked by the red dashed line in panel (a). The a-SNOM detects the evanescent electric field circled in red.

signal is demodulated at f_{tip}. The onset of the near-field signal appears at the same injection current as the far-field signal. The same is valid for the onset of the near-field signal demodulated at $2f_{tip}$ and $3f_{tip}$ (not shown).

Scanning the a-SNOM tip across the xy plane [axis orientation in Fig. 1(c)] yields the image of the evanescent electric field on the device surface. The results are shown in panels (a)–(e) of Fig. 2. Panel (a) shows an atomic-force microscope top view of the measured device.

The a-SNOM measurements reveal three operating regimes. For injection currents below laser threshold [panel (b), *thermal regime*] the near field is dominated by the material thermal emission.[14] At threshold [panel (c), *intermediate regime*], the thermal emission is still observable, but a near-field signal appears on the ridge top surface. Well above threshold [panel (d), *laser regime*] the intensity of the near-field signal increases by few orders of magnitude and it masks the thermal emission. A high resolution closeup [panel (e)] allows the clear observation of the standing wave, whose periodicity is found to be ≈1.25 μm. Note that even though the laser spectrum is multimode, the beating between the modes cannot be detected with the a-SNOM because of the reduced scanning range. The effective light wavelength inside the semiconductor material is $\lambda_{eff}=2.5$ μm, as obtained from the measured periodicity of the standing wave [Fig. 2(e)]. Alternatively, λ_{eff} can be inferred from the laser Fabry-Pérot emission spectrum. If the index dispersion is neglected, a value of 2.28 μm is obtained, in fair agreement with the value directly measured with the a-SNOM. The difference between the two values needs to be elucidated, but it might be ascribed to the index dispersion.

Two-dimensional (2D) numerical simulations,[19] allow a clearer understanding of the results. Figure 3(a) shows the electric field distribution (E_z component, i.e., transverse magnetic) for the air-guided mode under consideration superimposed onto a schematic view of the laser resonator. As detailed in Ref. 4, the laser mode is guided at the semiconductor-air interface, with an evanescent tail penetrating in the air cladding above [see Fig. 3(b)]. This is the field which is detected by the a-SNOM. It reflects the Fabry-Pérot structure of the guided wave inside the semiconductor laser, and it allows one to image the cavity standing waves, as shown in Fig. 3.

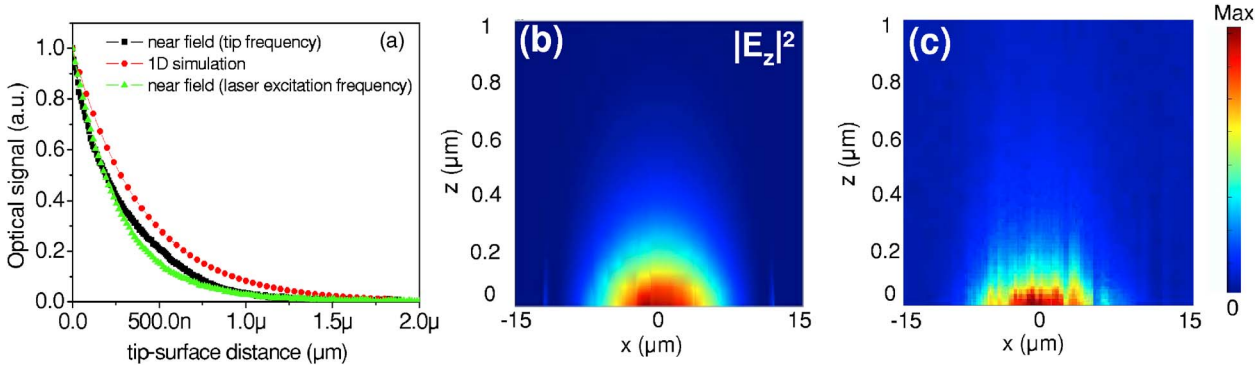

FIG. 4. (Color online) (a) a-SNOM signal as a function of the tip-sample distance. Black squares: SNOM signal demodulated at the tip frequency. Green triangles: SNOM signal demodulated at the laser repetition rate (84 kHz). Red circles: 1D numerical simulation ($|E_z|^2$ is plotted). (b) 2D simulation of the electric field intensity ($|E_z|^2$ is plotted) across the *xz* plane above the device surface. (c) Experimental near-field intensity measured by scanning the a-SNOM tip on the *xz* plane above the device surface. The agreement with the numerical simulation [panel (b)] is excellent.

Figure 4, panel (a), reports the near-field signal as a function of the tip-surface distance, with the tip kept at a fixed position in the *xy* plane. The signal has been demodulated at the tip frequency (black squares) or at the laser excitation repetition rate (green triangles). An exponential decay of the signal as a function of the tip-surface distance is observed, evidence of the evanescent nature of the electric field. The decay length of $|E_z|^2$ is ≈500 nm, in good agreement with one-dimensional (1D) numerical simulations (red circles). A more complete correspondence between theory and experiment can be obtained from the near-field signal across a 2D section in the *xz* plane above the laser surface [see Fig. 3(a) for axis orientations]. Figure 4(b) shows the result of numerical simulations ($|E_z|^2$ is plotted). The field has a maximum at the center of the ridge ($x=0$), and it vanishes on the sides where the semiconductor is covered by the metal contacts. In the *z* direction the field exhibits an exponential decay. The corresponding experimental measurement is reported in Fig. 4(c).

Finally, the average magnitude $|E|$ of the electric field at the laser surface can be estimated knowing the detector response, the numerical apertures of the detection system, and the tip scattering efficiency. To prevent degradation of the active region of the QC laser by the tip, the SNOM measurements are performed with tips with a large radius of curvature (≈200 nm). If the tip of the a-SNOM is approximated by a 200 nm radius tungsten sphere, a value of the field scattered by the tip $E_{\mathrm{scat}} \sim 3\times 10^7$ V/m is obtained. Because field amplification occurs at the tip apex,[20] $|E|$ is expected to be about two to three orders of magnitude lower than $|E_{\mathrm{scat}}|$, placing its value in the $3\times 10^4 - 3\times 10^5$ V/m range. This only constitutes a rough estimate because the scattering cross section of the tip strongly depends on its size and geometry, which are not known in detail.[20,21] However, the value found is consistent with the estimate which can be derived from the calculation of the energy stored in the laser cavity, which yields approximately 2×10^4 V/m.

In conclusion, we have employed a mid-IR a-SNOM to image the evanescent electric field on top of a $\lambda = 7.7$ μm QC laser. Future experiments will target fundamental as well as applicative aspects. Amongst the many possible developments, the combination of mid-IR near-field microscopy and surface-plasmon QC lasers offers the opportunity to elucidate the properties of surface plasmons on patterned metal structures[18] at frequencies very far from the metal plasma frequency.

The authors thank O. Painter, R. Perahia F. Julien, and C. Sirtori for useful discussions. One of the authors (P.-A.L.) acknowledges the Délégation Générale de l'Armement for financial support. This work was conducted as part of a EURYI scheme award. See www.esf.org/euryi. Two of the authors (V.M. and P.-A.L.) contributed equally to this work.

[1] F. K. Tittel, Y. Bakhirkin, A. A. Kosterev, and G. Wysocki, Rev. Laser Eng. **34**, 275 (2006).
[2] C. Gmachl, F. Capasso, D. L. Sivco, and A. Y. Cho, Rep. Prog. Phys. **64**, 1533 (2001).
[3] L. Diehl, B. G. Lee, P. Behroozi, M. Loncar, M. A. Belkin, F. Capasso, T. Aellen, D. Hofstetter, M. Beck, and J. Faist, Opt. Express **14**, 11660 (2006).
[4] V. Moreau, M. Bahriz, R. Colombelli, R. Perahia, O. Painter, A. Krysa, and L. R. Wilson, Opt. Express (submitted).
[5] R. Perahia, O. Painter, V. Moreau, and R. Colombelli, (unpublished).
[6] D. Hofstetter, T. Aellen, M. Beck, and J. Faist, IEEE Photonics Technol. Lett. **12**, 1610 (2000).
[7] W. Schrenk, N. Finger, S. Gianordoli, L. Hvozdara, G. Strasser, and E. Gornik, Appl. Phys. Lett. **77**, 2086 (2000).
[8] F. Zenhauser, M. P. O'Boyle, and H. K. Wikramasynghe, Appl. Phys. Lett. **65**, 1623 (1994).
[9] A. Lahrech, R. Bachelot, P. Gleyzes, and A.-C. Boccara, Opt. Lett. **21**, 1315 (1996).
[10] H.-T. Chen, R. Kersting, and G. C. Cho, Appl. Phys. Lett. **83**, 3009 (2003).
[11] G. Wurtz, R. Bachelot, and P. Royer, Eur. Phys. J.: Appl. Phys. **5**, 269 (1999).
[12] F. Chen, A. Itagi, J. A. Bain, D. D. Stancil, T. E. Schlesinger, L. Stebounova, G. C. Walker, and B. B. Akhremitchev, Appl. Phys. Lett. **83**, 3245 (2003).
[13] B. Knoll, F. Keilmann, A. Kramer, and R. Guckenberger, Appl. Phys. Lett. **70**, 2667 (1997).
[14] Y. De Wilde, F. Formanek, R. Carminati, B. Gralak, P.-A. Lemoine, K. Joulain, J.-P. Mulet, Y. Chen, and J.-J. Greffet, Nature (London) **444**, 740 (2006).
[15] E. Cubukcu, E. A. Kort, K. B. Crozier, and F. Capasso, Appl. Phys. Lett. **89**, 093120 (2006).
[16] B. Knoll and F. Keilmann, Nature (London) **399**, 134 (1999).
[17] M. Bahriz, V. Moreau, J. Palomo, R. Colombelli, D. A. Austin, J. W. Cockburn, L. R. Wilson, A. B. Krysa, and J. S. Roberts, Appl. Phys. Lett. **88**, 181103 (2006).
[18] S. Maier, S. R. Andrews, L. Martín-Moreno, F. J. Garcia-Vidal, Phys. Rev. Lett. **97**, 176805 (2006), and references therein.
[19] The finite-element simulations were performed with the commercial software COMSOL MULTIPHYSICS.
[20] B. Knoll and F. Keilmann, Opt. Commun. **182**, 321 (2000).
[21] F. Formanek, Y. De Wilde, and L. Aigouy, Ultramicroscopy **103**, 133 (2005).